



CHALMERS
UNIVERSITY OF TECHNOLOGY

Nonclassical Exciton Diffusion in Monolayer WSe₂

Downloaded from: <https://research.chalmers.se>, 2024-06-11 15:14 UTC

Citation for the original published paper (version of record):

Wagner, K., Zipfel, J., Rosati, R. et al (2021). Nonclassical Exciton Diffusion in Monolayer WSe₂. Physical Review Letters, 127(7). <http://dx.doi.org/10.1103/PhysRevLett.127.076801>

N.B. When citing this work, cite the original published paper.

Nonclassical Exciton Diffusion in Monolayer WSe₂

Koloman Wagner¹, Jonas Zipfel^{1,2}, Roberto Rosati³, Edith Wietek¹, Jonas D. Ziegler¹, Samuel Brem³, Raúl Perea-Causín⁴, Takashi Taniguchi⁵, Kenji Watanabe⁶, Mikhail M. Glazov⁷, Ermin Malic^{4,3}, and Alexey Chernikov^{1,8,*}

¹Department of Physics, University of Regensburg, Regensburg D-93053, Germany

²Molecular Foundry, Lawrence Berkeley National Laboratory, Berkeley, California 94720, USA

³Department of Physics, Philipps-Universität Marburg, Renthof 7, Marburg D-35032, Germany

⁴Department of Physics, Chalmers University of Technology, Fysikgården 1, 41258 Gothenburg, Sweden

⁵International Center for Materials Nanoarchitectonics, National Institute for Materials Science, Tsukuba, Ibaraki 305-004, Japan

⁶Research Center for Functional Materials, National Institute for Materials Science, Tsukuba, Ibaraki 305-004, Japan

⁷Ioffe Institute, 194021 Saint Petersburg, Russian Federation

⁸Dresden Integrated Center for Applied Physics and Photonic Materials (IAPP) and Würzburg-Dresden Cluster of Excellence *ct.qmat*, Technische Universität Dresden, 01062 Dresden, Germany

 (Received 9 February 2021; accepted 24 June 2021; published 9 August 2021)

We experimentally demonstrate time-resolved exciton propagation in a monolayer semiconductor at cryogenic temperatures. Monitoring phonon-assisted recombination of dark states, we find a highly unusual case of exciton diffusion. While at 5 K the diffusivity is intrinsically limited by acoustic phonon scattering, we observe a pronounced *decrease* of the diffusion coefficient with increasing temperature, far below the activation threshold of higher-energy phonon modes. This behavior corresponds neither to well-known regimes of semiclassical free-particle transport nor to the thermally activated hopping in systems with strong localization. Its origin is discussed in the framework of both microscopic numerical and semiphenomenological analytical models illustrating the observed characteristics of nonclassical propagation. Challenging the established description of mobile excitons in monolayer semiconductors, these results open up avenues to study quantum transport phenomena for excitonic quasiparticles in atomically thin van der Waals materials and their heterostructures.

DOI: 10.1103/PhysRevLett.127.076801

Correlated motion of Coulomb-bound electron-hole pairs, commonly known as excitons [1,2], represents a vibrant field of research. From their electronic constituents excitons naturally inherit the ability to propagate through the crystal [3,4]. Moreover, optically active excitons can directly visualize transport phenomena and possess emerging properties associated with interacting, composite bosons [5], including discussions of superfluidity [6,7], condensation [8], phonon wind [9], and ring formation [10]. Particularly interesting in this context are layered two-dimensional (2D) materials [11] such as semiconducting transition-metal dichalcogenides (TMDCs) [12–15]. As monolayers they host robust exciton states with high binding energies [16,17] and the possibility to carry spin-valley information quanta [18–20]. The excitons in TMDCs have been shown to be mobile [21–28], guided by gradients [29–31], exhibit nonlinear diffusion [32–37], strain dependence [38], as well as intriguing propagation in heterostructures [39–42].

In general, systems hosting mobile excitons such as TMDCs fall into two main categories, exhibiting either semiclassical free-particle transport [43–45] or hopping between localization sites [46,47]. These mechanisms are

typical for Wannier-Mott excitons with spatially extended wave functions in inorganic semiconductors and tightly bound Frenkel-like states in molecular crystals, respectively. Excitons in TMDC monolayers, however, present a particularly interesting, intermediate case. They uniquely combine the characteristics of the two descriptions, with wave functions being delocalized across many unit cells but also exhibiting high binding energies [17]. This duality is expected to manifest itself prominently in the exciton transport behavior, including potential emergence of quantum interference phenomena [48–52]. Despite much progress, however, only little is known regarding the appropriate picture for the exciton propagation in monolayer semiconductors, currently based on the assumption of a purely semiclassical framework [22,24,28,30,32,33,36,37,53].

Here, we address the question of the fundamental description of mobile excitons in 2D TMDCs, demonstrating the unusual nature of the exciton diffusion in these systems. In the experiments, we take advantage of dark excitons in hBN-encapsulated WSe₂ monolayers with suppressed long-range disorder [26]. In contrast to bright excitons with picosecond lifetimes [54], dark states live up

to hundreds of ps [55,56] and allow us to study them under thermal equilibrium conditions. Dark exciton emission is monitored through phonon-assisted recombination channels [57–63] via temporally and spatially resolved microscopy at cryogenic temperatures after weak, strictly resonant excitation of the bright state. Importantly, the characteristic spectral shape of the phonon sidebands (PSBs) [4,58,61] allows for an independent evaluation of the exciton temperature and scattering rates, making it possible to extract key parameters governing exciton propagation from experiments.

At the lowest studied temperature of 5 K, we detect linear diffusion with a coefficient of $2.4 \pm 0.5 \text{ cm}^2/\text{s}$, essentially limited by the exciton-phonon coupling. As the temperature increases, we observe an unusually strong *decrease* already in the low-temperature range of 4 to 30 K, far below activation threshold of high-energy phonons. Under these conditions, the observations agree neither with the semiclassical free-particle description nor with thermally activated hopping. These conclusions are further supported by quantitative analysis involving experimentally determined scattering rates as well as many-body calculations of the spatiotemporal exciton dynamics. In view of the recently predicted quantum interference phenomena for TMDC monolayers [52], it allows us to experimentally demonstrate an interesting scenario that requires nonclassical effects in the exciton transport.

The studied hBN-encapsulated WSe₂ monolayers were obtained by mechanical exfoliation and stamping [64] of bulk crystals (WSe₂ from “HQgraphene,” hBN from NIMS) onto SiO₂/Si substrates (see Supplemental Material [65]). For the measurements the samples were placed in a microscopy cryostat. We used a 80 MHz, 140 fs-pulsed Ti:sapphire as excitation source, tuned into resonance with the bright exciton X_0 at 1.726 eV to minimize excess energy and avoid contributions of unbound electron-hole pairs. The incident light was focused to a spot with about 1 μm diameter. The emission was collected from a lateral cross section and guided through an imaging spectrometer equipped with a mirror and a grating to provide spatial and spectral resolutions, respectively. We employed a streak camera for time-resolved detection and a CCD-sensor for time-integrated signals; also see Refs. [28,33].

The optical fingerprints used to monitor dark excitons in WSe₂ monolayer are schematically illustrated in Fig. 1(a). The short-lived, bright exciton transition ($K - K$) is denoted by the respective valence and conduction band valleys of the empty and filled electron states that form the exciton. The schematic and the notation are chosen from the K valley perspective and apply equally for K' . After optical injection, bright excitons rapidly redistribute toward lower-lying states [55,62,91]. These are commonly labeled as *dark excitons* [55] due to strongly suppressed light-matter coupling from either nonzero spin (*intravalley*

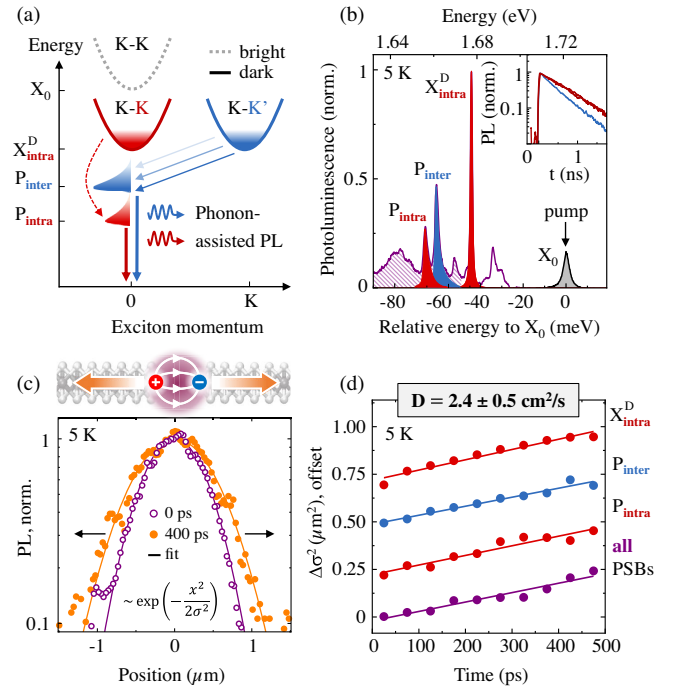


FIG. 1. (a) Schematic illustration of the relevant phonon-assisted emission of dark excitons in WSe₂. (b) Typical luminescence spectrum of hBN-encapsulated WSe₂ monolayer at $T = 5 \text{ K}$, after resonant excitation of X_0 . Colored areas schematically indicate individual components. Corresponding PL transients are presented in the inset. (c) Representative spatially resolved profiles of the dark exciton PSBs at 0 and 400 ps after resonant excitation of X_0 . (d) Mean squared displacement of the individually measured PL signatures as function of time. Data are vertically offset for clarity.

$K - K$ triplets) or large center-of-mass momentum (*intervalley* $K - K'$ singlets).

While being essentially dark in absorption, these states can be detected in photoluminescence (PL) at sufficiently low temperatures [17]. Intravalley triplets couple weakly to light via out-of-plane-polarization [56,92] and are observed with large collection apertures. They give rise to the prominent X_{intra}^D transition in the PL spectrum at $T = 5 \text{ K}$, presented in Fig. 1(b). In addition, they couple to the in-plane polarization through a phonon-assisted process [59,60,63] leading to the emergence of the P_{intra} sideband, indicated in Figs. 1(a) and 1(b). Similarly, intervalley $K - K'$ singlets recombine under emission of zone-edge phonons [61–63] and exhibit PL labeled as P_{inter} , while their direct recombination is forbidden due to momentum conservation. Additional, weak signatures stem largely from the higher order PSBs below P_{intra} , a feature attributed to the $K - \Lambda$ sideband at about -50 meV [61,62], nearly negligible PL from negative trions (-31 and -38 meV) as well as a peak at -35 meV , consistent with Refs. [59,60,63].

Importantly, all dark states are long lived with population lifetimes τ_X of 500 and 800 ps for P_{inter} and P_{intra} (X_{intra}^D),

respectively, as illustrated in the inset of Fig. 1(b) (also see Supplemental Material [65]). Following resonant excitation of the bright state, relaxation and cooling of dark excitons occur on much shorter timescales, during the first tens of ps [62]. During their lifetimes of many hundreds of ps, these excitons should be thus thermally equilibrated within their respective intra- and intervalley subsets.

Representative profiles of the spatially resolved dark state emission are presented in Fig. 1(c) for 0 and 400 ps after the excitation at $T = 5$ K. They illustrate broadening of the spatial exciton distribution over time. The employed excitation density of 50 nJ cm^{-2} corresponds to the linear regime with the estimated electron-hole pair density of several 10^{10} cm^{-2} per pulse. For the quantitative analysis we fit the PL profiles with a Gauss function, $\propto \exp[-x^2/2\sigma^2(t)]$, where x is the coordinate along the detected cross section. From this procedure we extract time-dependent change of the variance $\Delta\sigma^2(t) = \sigma^2(t) - \sigma^2(0)$, commonly labeled as the mean squared displacement. Corresponding values, obtained from the individual, spectrally filtered emission features of the dark states, are presented in Fig. 1(d). All of them exhibit very similar behavior with the linear increase of $\Delta\sigma^2$ over time being a clear hallmark of diffusive propagation [11]. From $\Delta\sigma^2(t) = 2Dt$ we extract an average diffusion coefficient $D = 2.4 \pm 0.5 \text{ cm}^2/\text{s}$, corresponding to diffusion lengths $\sqrt{2D\tau_X}$ on the order of $0.5 \mu\text{m}$.

According to the semiclassical description [44], the diffusion coefficient is determined by the total mass M_X (that is about 0.75 of the free electron mass m_0 for dark excitons in WSe_2 [93]), temperature T , and the scattering rate τ_s^{-1} :

$$D = \frac{k_B T \tau_s}{M_X}, \quad (1)$$

where k_B denotes the Boltzmann constant. Ideally, the primary mechanism limiting the diffusion at low temperatures is the quasielastic exciton scattering with long-wavelength acoustic phonons. The corresponding rate scales linearly with the temperature and is expected to yield a temperature-independent, constant diffusivity for the purely semi-classical behavior [52]. To elucidate the nature of the exciton transport it is thus necessary to gain independent access to both diffusion coefficient and scattering rate τ_s^{-1} as functions of the exciton temperature. As we demonstrate in the following, the rates and the temperatures are directly obtained from spectrally resolved, characteristic PSB profiles. That also allows us to confirm the equilibrated state of the photoexcited exciton system.

PL spectra in the temperature range between 5 and 50 K are presented in Figs. 2(a) and 2(b) for the PSBs and the X_{intra}^D peak, respectively. In order to fulfill both momentum and energy conservation, the direct radiative transition is only allowed for vanishing momenta and near-zero

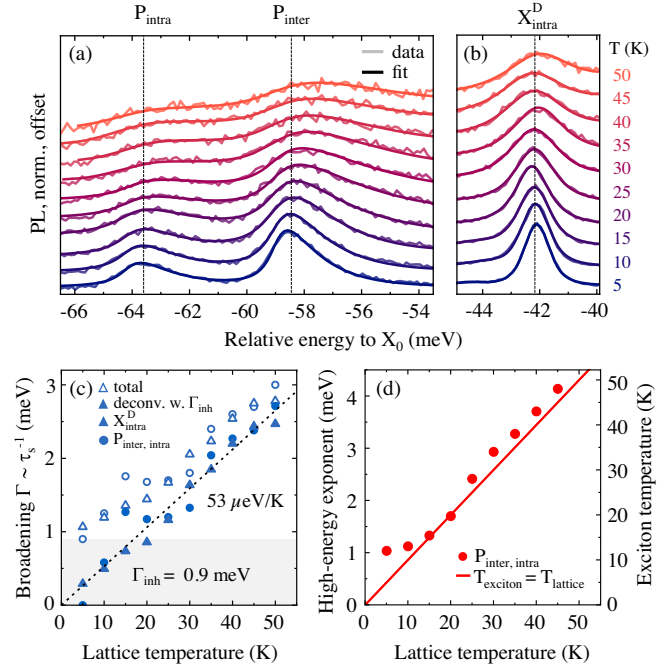


FIG. 2. (a) PL spectra of dark exciton PSBs after resonant, pulsed excitation. (b) PL spectra of the intravalley dark exciton zero-phonon line. (c) Extracted symmetric peak broadening component (full-width-at-half-maximum) representing the temperature-dependent scattering rate. (d) High-energy exponent representing the exciton temperature.

kinetic energies. It results in a fully symmetric X_{intra}^D peak that motivates the use of a Voigt profile with a temperature-dependent linewidth Γ for analysis. In contrast to that, recombination via phonon-assisted emission can involve excitons with arbitrary large center-of-mass momenta. This yields the typically asymmetric shape of the sidebands, directly reflecting the exciton distribution in momentum space [4,94,95], as illustrated in Fig. 1(a). To fit the observed PSBs we thus convolute a Lorentzian peak with an exponential high-energy flank $\propto \exp[-E/k_B T_X]$ (see Supplemental Material [65]). The symmetric broadening then accounts for the scattering rate τ_s^{-1} and the asymmetric flank represents the exciton distribution in kinetic energy, corresponding to an effective temperature T_X .

As shown in Figs. 2(a) and 2(b), this choice of the fit functions describes the data very well, allowing for a meaningful extraction of the parameters. Temperature-dependent broadening is presented in Fig. 2(c) as both total and deconvoluted linewidths. For the latter we assume an additional, constant broadening of 0.9 meV to account for residual, spatially extended inhomogeneities. The observed linear increase of the linewidth with a coefficient of $53 \mu\text{eV/K}$ is characteristic for quasielastic scattering with phonons from the linear acoustic branch [96–98] (see Supplemental Material [65] for additional discussion). In this case, each phonon-scattering event randomly changes

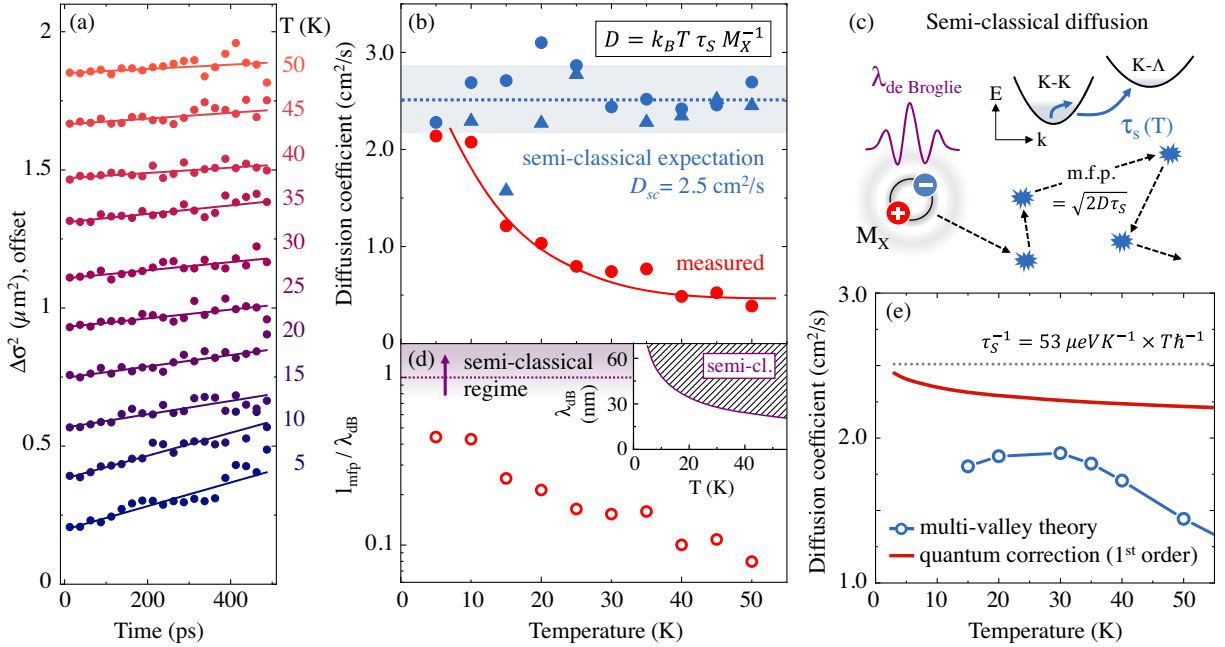


FIG. 3. (a) Transient mean squared displacement of the spatial exciton distribution for temperatures between 5 and 50 K. Data are vertically offset for clarity. (b) Measured diffusion coefficients in comparison to the semiclassical expectation from Eq. (1) based on the measured scattering rates, Fig. 2(c). The shaded area and the lines are guides to the eye. (c) Illustration of the semiclassical exciton propagation and scattering via thermally activated phonon absorption. (d) Temperature-dependent ratio of the mean free path corresponding to measured diffusion coefficients and the de Broglie wavelength of the excitons. Absolute values for the latter are given in the inset. (e) Exciton diffusivity calculated using a microscopic multivalley model in a semiclassical framework and the influence of quantum corrections.

the propagation direction of the exciton wave packet. The *optical phase* scattering rate determining the spectral broadening is then equal to that for *momentum* scattering governing the diffusion in Eq. (1). Moreover, the broadening obtained from the symmetric component of the PSBs is nearly identical to that of the X_{intra}^D peak, supporting the consistency of the applied model. Finally, the extracted exciton temperature presented in Fig. 2(d) corresponds to that of the lattice with only small deviations.

To illustrate temperature-dependent diffusion, time-dependent expansion of the spatially resolved PL profiles is presented in Fig. 3(a) for a series of temperatures up to 50 K. Here, we detect the accumulated signal of all sidebands taking advantage of an enhanced signal-to-noise ratio and spectrally independent diffusion coefficients (cf. Fig. 1). The extracted diffusivity is shown in Fig. 3(b) as a function of temperature. At lowest temperatures the measured values are close to the semiclassical expectation $D_{\text{sc}} = 2.5 \text{ cm}^2/\text{s}$ using the measured broadening coefficient of $53 \mu\text{eV}/\text{K}$ and Eq. (1). As the temperature increases, we do not observe any thermally activated increase of diffusion that would otherwise point to hopping [47] or defect-assisted scattering [99,100]. Instead, we find a pronounced *decrease* of the diffusivity already during the first tens of K.

This peculiar observation strongly contrasts the expectation of a constant diffusivity from the semiclassical model,

Eq. (1), using independently determined scattering rates from Fig. 2(c), shown for direct comparison. Importantly, the general description via Eq. (1) does not depend on a specific origin of the scattering. We further emphasize the absence of nonequilibrium effects due to the long time-scales in our observations, far beyond the initial relaxation during the first tens of ps [62]. Finally, our findings are robust, confirmed using a sample in the neutral-doping regime, and do not depend on the excitation density (see Supplemental Material [65]). The latter allows us to exclude nonlinearities, such as bimolecular processes [33,101] or phonon-wind effects [35,102].

The observed inadequacy of the semiclassical description can be rationalized in view of the formal applicability limit, known as the Mott-Ioffe-Regel criterion [103]. In the semiclassical picture, schematically illustrated in Fig. 3(c), the exciton diffusion is dictated by temperature and scattering rate τ_s^{-1} . The model is expected to break down when the mean-free-path $l_{\text{mfp}} = \sqrt{2D\tau_s}$ of the particle becomes similar or smaller than the wave packet size characterized by the de Broglie wavelength $\lambda_{\text{dB}} = \sqrt{2\pi\hbar(M_X k_B T)^{-1/2}}$. From the scattering rates in Fig. 2(c) we indeed obtain $l_{\text{mfp}} \approx \lambda_{\text{dB}}$ for all studied temperatures. We also present the ratio between l_{mfp} , extracted from measured diffusion coefficients under the assumption of Eq. (1), and λ_{dB} in Fig. 3(d). This ratio decreases far below unity at elevated temperatures, further illustrating the

inconsistency of the semiclassical description. Moreover, due to the similarity of the key exciton parameters and scattering rates, the above considerations should apply for other TMDC monolayers as well.

It is thus instructive to consider current theoretical understanding of the exciton transport in 2D TMDCs both in a semiclassical framework with a more comprehensive description of the exciton band structure and from the perspective of quantum corrections. For this purpose, the results of the calculations for the exciton diffusivity in thermal equilibrium are presented in Fig. 3(e). In the multivalley approach we use a model Hamiltonian in the excitonic basis, including carrier-light, carrier-phonon, and carrier-carrier interactions to set up equations of motion for the excitons [36,38,62]. The required input parameters for monolayer WSe₂ are taken from first-principle studies [93,104]. The diffusion coefficient is extracted from the spatiotemporal evolution of the excitons in the semiclassical approximation neglecting exciton-exciton mechanisms [36–38]. The model takes explicitly into account both a realistic multivalley band structure of WSe₂ and the exciton-phonon coupling beyond the long-wavelength acoustic branches. In particular, we include thermal activation of higher-energy phonon absorption that leads to additional intervalley scattering for excitons, schematically illustrated in Fig. 3(c). At low temperatures we find an essentially constant value of the diffusion coefficient, close to the experimental result at 5 K and the semiclassical estimation via Eq. (1). Only above about 30 K the model predicts a small decrease of the diffusivity. This onset depends on the energy of the phonons involved in the intervalley scattering and, most importantly, is always accompanied by a nonlinear increase of the linewidth (cf. Supplemental Material [65] and Ref. [98]).

First-order quantum corrections to a simplified semiclassical picture of constant diffusivity are illustrated in Fig. 3(e). Recently developed for 2D TMDCs [52], the calculations are adapted for the WSe₂ monolayer by using the exciton mass and the sound velocity of $0.75m_0$ and 3.3 km/s, respectively. The model accounts perturbatively for quantum interference effects in the exciton transport. Constructive interference can arise between clock- and counterclockwise propagation of exciton wave packets through closed loops, leading to an effective localization of excitons (also see Supplemental Material [65]). For quasielastic exciton-phonon interaction [52], the specific interplay between the loss of the *relative* phase in the loop and momentum scattering results in an initial *decrease* of the effective diffusivity with increasing temperature. Interestingly, the functional form of the quantum corrections and their temperature dependence indeed resemble experimental observations. However, the magnitude of the measured effect is almost an order of magnitude higher. It follows that while nonclassical contributions to the exciton diffusion are clearly necessary, further development of the

theory beyond the commonly studied first order in $\hbar/(k_B T \tau_s)$ quantum corrections is required.

In conclusion, we have explored the nature of the exciton transport in monolayer semiconductors via transient microscopy at cryogenic temperatures. The excitons are found to exhibit neither the characteristic behavior of diffusive free particle propagation nor that of thermally activated hopping between localized states. Measured diffusion coefficients strongly deviate from the semiclassical expectation of a temperature-independent diffusivity based on independently obtained momentum scattering rates. Instead, we find evidence for nonclassical effects playing a key role, consistent with comparable scales of the free propagation and de Broglie lengths. The obtained results should be relevant for optoelectronic devices based on mobile optical excitations in 2D materials and provide a solid platform to understand exciton propagation in more complex heterostructures that involve monolayers as building blocks. The observed unusual behavior in the exciton diffusion highlights van der Waals monolayer semiconductors as a particularly promising platform to merge the rich field of quantum transport phenomena with the physics of composite excitonic quasiparticles.

We thank Alexander Högele and Victor Funk for fruitful discussions as well as Christian Bäuml and Nicola Paradiso for their assistance with pre-patterned substrate preparation. Financial support by the DFG via Emmy Noether Initiative (CH 1672/1), SFB 1277 (project B05), as well as the Würzburg-Dresden Cluster of Excellence on Complexity and Topology in Quantum Matter ct.qmat (EXC 2147) and SFB 1083 (project B09) is gratefully acknowledged. The theoretical part of the work by R. R., S. B., R. P.-C., and E. M. was further supported by the European Union's Horizon 2020 research and innovation program under Grant Agreement No. 881603. The computations were enabled by resources provided by the Swedish National Infrastructure for Computing (SNIC) at C3SE and HPC2N. We acknowledge the funding provided by 2D TECH VINNOVA competence Center (Ref. 2019-00068). K. Watanabe and T. T. acknowledge support from the Elemental Strategy Initiative, conducted by the MEXT, Japan, Grant No. JPMXP0112101001, JSPS KAKENHI Grant No. JP20H00354 and the CREST (JPMJCR15F3), JST. The development of the analytical theory by M. M. G. has been supported by RSF Project No. 19-12-00051.

*alexey.chernikov@tu-dresden.de

- [1] J. Frenkel, *Phys. Rev.* **37**, 17 (1931).
- [2] E. F. Gross and N. A. Karrjew, *Dokl. Akad. Nauk SSSR* **84**, 471 (1952).
- [3] E. L. Ivchenko, *Optical Spectroscopy of Semiconductor Nanostructures* (Alpha Science, Harrow England, 2005).
- [4] C. Klingshirn, *Semiconductor Optics*, 3rd ed. (Springer, Berlin Heidelberg New York, 2007).

- [5] H. Haug and S. W. Koch, *Quantum Theory of the Optical and Electronic Properties of Semiconductors*, 5th ed. (World Scientific, Singapore, 2009).
- [6] A. Mysyrowicz, E. Benson, and E. Fortin, *Phys. Rev. Lett.* **77**, 896 (1996).
- [7] E. Benson, E. Fortin, and A. Mysyrowicz, *Solid State Commun.* **101**, 313 (1997).
- [8] S. A. Moskalenko and D. W. Snoke, *Bose-Einstein Condensation of Excitons and Biexcitons* (Cambridge University Press, Cambridge, England, 2005).
- [9] S. Tikhodeev, G. Kopelevich, and N. Gippius, *Phys. Status Solidi* **206**, 45 (1998).
- [10] L. V. Butov, L. S. Levitov, A. V. Mintsev, B. D. Simons, A. C. Gossard, and D. S. Chemla, *Phys. Rev. Lett.* **92**, 117404 (2004).
- [11] N. S. Ginsberg and W. A. Tisdale, *Annu. Rev. Phys. Chem.* **71**, 1 (2020).
- [12] J. Wilson and A. Yoffe, *Adv. Phys.* **18**, 193 (1969).
- [13] K. S. Novoselov, D. Jiang, F. Schedin, T. J. Booth, V. V. Khotkevich, S. V. Morozov, and A. K. Geim, *Proc. Natl. Acad. Sci. U.S.A.* **102**, 10451 (2005).
- [14] K. F. Mak, C. Lee, J. Hone, J. Shan, and T. F. Heinz, *Phys. Rev. Lett.* **105**, 136805 (2010).
- [15] A. Splendiani, L. Sun, Y. Zhang, T. Li, J. Kim, C.-Y. Chim, G. Galli, and F. Wang, *Nano Lett.* **10**, 1271 (2010).
- [16] J. Xiao, M. Zhao, Y. Wang, and X. Zhang, *Nanophotonics* **6**, 1309 (2017).
- [17] G. Wang, A. Chernikov, M. M. Glazov, T. F. Heinz, X. Marie, T. Amand, and B. Urbaszek, *Rev. Mod. Phys.* **90**, 021001 (2018).
- [18] X. Xu, W. Yao, D. Xiao, and T. F. Heinz, *Nat. Phys.* **10**, 343 (2014).
- [19] H. Yu, X. Cui, X. Xu, and W. Yao, *Natl. Sci. Rev.* **2**, 57 (2015).
- [20] M. M. Glazov and L. E. Golub, *Phys. Rev. Lett.* **125**, 157403 (2020).
- [21] N. Kumar, Q. Cui, F. Ceballos, D. He, Y. Wang, and H. Zhao, *Phys. Rev. B* **89**, 125427 (2014).
- [22] T. Kato and T. Kaneko, *ACS Nano* **10**, 9687 (2016).
- [23] L. Yuan, T. Wang, T. Zhu, M. Zhou, and L. Huang, *J. Phys. Chem. Lett.* **8**, 3371 (2017).
- [24] F. Cadiz, C. Robert, E. Courtade, M. Manca, L. Martinelli, T. Taniguchi, K. Watanabe, T. Amand, A. C. H. Rowe, D. Paget, B. Urbaszek, and X. Marie, *Appl. Phys. Lett.* **112**, 152106 (2018).
- [25] Y. Fu, D. He, J. He, A. Bian, L. Zhang, S. Liu, Y. Wang, and H. Zhao, *Adv. Mater. Interfaces* **6**, 1901307 (2019).
- [26] A. Raja, L. Waldecker, J. Zipfel, Y. Cho, S. Brem, J. D. Ziegler, M. Kulig, T. Taniguchi, K. Watanabe, E. Malic, T. F. Heinz, T. C. Berkelbach, and A. Chernikov, *Nat. Nanotechnol.* **14**, 832 (2019).
- [27] S. Z. Uddin, H. Kim, M. Lorenzon, M. Yeh, D.-H. Lien, E. S. Barnard, H. Htoon, A. Weber-Bargioni, and A. Javey, *ACS Nano* **14**, 13433 (2020).
- [28] J. Zipfel, M. Kulig, R. Perea-Causín, S. Brem, J. D. Ziegler, R. Rosati, T. Taniguchi, K. Watanabe, M. M. Glazov, E. Malic, and A. Chernikov, *Phys. Rev. B* **101**, 115430 (2020).
- [29] D. F. Cordovilla Leon, Z. Li, S. W. Jang, C.-H. Cheng, and P. B. Deotare, *Appl. Phys. Lett.* **113**, 252101 (2018).
- [30] V. Shahnazaryan, O. Kyriienko, and H. Rostami, *Phys. Rev. B* **100**, 165303 (2019).
- [31] S. Hao, M. Z. Bellus, D. He, Y. Wang, and H. Zhao, *Nanoscale Horiz.* **5**, 139 (2020).
- [32] S. Mouri, Y. Miyauchi, M. Toh, W. Zhao, G. Eda, and K. Matsuda, *Phys. Rev. B* **90**, 155449 (2014).
- [33] M. Kulig, J. Zipfel, P. Nagler, S. Blanter, C. Schüller, T. Korn, N. Paradiso, M. M. Glazov, and A. Chernikov, *Phys. Rev. Lett.* **120**, 207401 (2018).
- [34] J. Wang, Y. Guo, Y. Huang, H. Luo, X. Zhou, C. Gu, and B. Liu, *Appl. Phys. Lett.* **115**, 131902 (2019).
- [35] M. M. Glazov, *Phys. Rev. B* **100**, 045426 (2019).
- [36] R. Perea-Causín, S. Brem, R. Rosati, R. Jago, M. Kulig, J. D. Ziegler, J. Zipfel, A. Chernikov, and E. Malic, *Nano Lett.* **19**, 7317 (2019).
- [37] R. Rosati, R. Perea-Causín, S. Brem, and E. Malic, *Nanoscale* **12**, 356 (2020).
- [38] R. Rosati, S. Brem, R. Perea-Causín, R. Schmidt, I. Niehues, S. Michaelis de Vasconcellos, R. Bratschitsch, and E. Malic, *2D Mater.* **8**, 015030 (2021).
- [39] P. Rivera, K. L. Seyler, H. Yu, J. R. Schaibley, J. Yan, D. G. Mandrus, W. Yao, and X. Xu, *Science* **351**, 688 (2016).
- [40] E. V. Calman, M. M. Fogler, L. V. Butov, S. Hu, A. Mishchenko, and A. K. Geim, *Nat. Commun.* **9**, 1895 (2018).
- [41] D. Unuchek, A. Ciarrocchi, A. Avsar, K. Watanabe, T. Taniguchi, and A. Kis, *Nature (London)* **560**, 340 (2018).
- [42] L. Yuan, B. Zheng, J. Kunstmann, T. Brumme, A. B. Kuc, C. Ma, S. Deng, D. Blach, A. Pan, and L. Huang, *Nat. Mater.* **19**, 617 (2020).
- [43] L. M. Smith, D. R. Wake, J. P. Wolfe, D. Levi, M. V. Klein, J. Klem, T. Henderson, and H. Morkoç, *Phys. Rev. B* **38**, 5788 (1988).
- [44] J. Erland, B. S. Razbirin, K.-H. Pantke, V. G. Lyssenko, and J. M. Hvam, *Phys. Rev. B* **47**, 3582 (1993).
- [45] S. Grosse, R. Arnold, G. von Plessen, M. Koch, J. Feldmann, V. M. Axt, T. Kuhn, R. Rettig, and W. Stolz, *Phys. Status Solidi* **204**, 147 (1997).
- [46] P. W. Anderson, *Phys. Rev.* **109**, 1492 (1958).
- [47] O. V. Mikhnenko, P. W. M. Blom, and T.-Q. Nguyen, *Energy Environ. Sci.* **8**, 1867 (2015).
- [48] E. L. Ivchenko, G. E. Pikus, B. S. Razbirin, and A. I. Starukhin, *J. Exp. Theor. Phys.* **45**, 1172 (1977).
- [49] B. Altshuler and A. Aronov, in *Electron-Electron Interactions in Disordered Systems*, edited by A. L. Efros and M. Pollak (North Holland, Amsterdam, 1985).
- [50] P. I. Arseev and A. B. Dzyubenko, *J. Exp. Theor. Phys.* **87**, 200 (1998).
- [51] F. Evers and A. D. Mirlin, *Rev. Mod. Phys.* **80**, 1355 (2008).
- [52] M. M. Glazov, *Phys. Rev. Lett.* **124**, 166802 (2020).
- [53] M. G. Harats, J. N. Kirchhof, M. Qiao, K. Greben, and K. I. Bolotin, *Nat. Photonics* **14**, 324 (2020).
- [54] C. Robert, R. Picard, D. Lagarde, G. Wang, J. P. Echeverry, F. Cadiz, P. Renucci, A. Högele, T. Amand, X. Marie, I. C. Gerber, and B. Urbaszek, *Phys. Rev. B* **94**, 155425 (2016).
- [55] X.-X. Zhang, Y. You, Shu Yang Frank Zhao, and T. F. Heinz, *Phys. Rev. Lett.* **115**, 257403 (2015).

- [56] C. Robert, T. Amand, F. Cadiz, D. Lagarde, E. Courtade, M. Manca, T. Taniguchi, K. Watanabe, B. Urbaszek, and X. Marie, *Phys. Rev. B* **96**, 155423 (2017).
- [57] J. Lindlau, C. Robert, V. Funk, J. Förste, M. Förg, L. Colombier, A. Neumann, E. Courtade, S. Shree, T. Taniguchi, K. Watanabe, M. M. Glazov, X. Marie, B. Urbaszek, and A. Högele, [arXiv:1710.00988](https://arxiv.org/abs/1710.00988).
- [58] D. Christiansen, M. Selig, G. Berghäuser, R. Schmidt, I. Niehues, R. Schneider, A. Arora, S. M. de Vasconcellos, R. Bratschitsch, E. Malic, and A. Knorr, *Phys. Rev. Lett.* **119**, 187402 (2017).
- [59] C. Liu, H. Hong, Q. Wang, P. Liu, Y. Zuo, J. Liang, Y. Cheng, X. Zhou, J. Wang, Y. Zhao, J. Xiong, B. Xiang, J. Zhang, and K. Liu, *Nanoscale* **11**, 17195 (2019).
- [60] Z. Li, T. Wang, C. Jin, Z. Lu, Z. Lian, Y. Meng, M. Blei, S. Gao, T. Taniguchi, K. Watanabe, T. Ren, S. Tongay, L. Yang, D. Smirnov, T. Cao, and S.-F. Shi, *Nat. Commun.* **10**, 2469 (2019).
- [61] S. Brem, A. Ekman, D. Christiansen, F. Katsch, M. Selig, C. Robert, X. Marie, B. Urbaszek, A. Knorr, and E. Malic, *Nano Lett.* **20**, 2849 (2020).
- [62] R. Rosati, K. Wagner, S. Brem, R. Perea-Causín, E. Wietek, J. Zipfel, J. D. Ziegler, M. Selig, T. Taniguchi, K. Watanabe, A. Knorr, A. Chernikov, and E. Malic, *ACS Photonics* **7**, 2756 (2020).
- [63] M. He, P. Rivera, D. Van Tuan, N. P. Wilson, M. Yang, T. Taniguchi, K. Watanabe, J. Yan, D. G. Mandrus, H. Yu, H. Dery, W. Yao, and X. Xu, *Nat. Commun.* **11**, 618 (2020).
- [64] A. Castellanos-Gomez, M. Buscema, R. Molenaar, V. Singh, L. Janssen, H. S. J. van der Zant, and G. A. Steele, *2D Mater.* **1**, 011002 (2014).
- [65] See Supplemental Material at <http://link.aps.org/supplemental/10.1103/PhysRevLett.127.076801>, which includes Refs. [66–90], for additional experimental data, theoretical analysis, and discussion.
- [66] S. J. Byrnes, [arXiv:1603.02720](https://arxiv.org/abs/1603.02720).
- [67] Y. Li, A. Chernikov, X. Zhang, A. Rigosi, H. M. Hill, A. M. van der Zande, D. A. Chenet, E.-M. Shih, J. Hone, and T. F. Heinz, *Phys. Rev. B* **90**, 205422 (2014).
- [68] Y. You, X. Zhang, T. C. Berkelbach, M. S. Hybertsen, D. R. Reichman, and T. F. Heinz, *Nat. Phys.* **11**, 477 (2015).
- [69] Z. Ye, L. Waldecker, E. Y. Ma, D. Rhodes, A. Antony, B. Kim, X.-X. Zhang, M. Deng, Y. Jiang, Z. Lu, D. Smirnov, K. Watanabe, T. Taniguchi, J. Hone, and T. F. Heinz, *Nat. Commun.* **9**, 3718 (2018).
- [70] A. J. Goodman, D.-H. Lien, G. H. Ahn, L. L. Spiegel, M. Amani, A. P. Willard, A. Javey, and W. A. Tisdale, *J. Phys. Chem. C* **124**, 12175 (2020).
- [71] J. D. Ziegler, J. Zipfel, B. Meisinger, M. Menahem, X. Zhu, T. Taniguchi, K. Watanabe, O. Yaffe, D. A. Egger, and A. Chernikov, *Nano Lett.* **20**, 6674 (2020).
- [72] C. Robert, D. Lagarde, F. Cadiz, G. Wang, B. Lassagne, T. Amand, A. Balocchi, P. Renucci, S. Tongay, B. Urbaszek, and X. Marie, *Phys. Rev. B* **93**, 205423 (2016).
- [73] V. Chellappan, A. L. C. Pang, S. Sarkar, Z. E. Ooi, and K. E. J. Goh, *Electron. Mater. Lett.* **14**, 766 (2018).
- [74] J. Olivero and R. L. Longbothum, *J. Quant. Spectrosc. Radiat. Transfer* **17**, 233 (1977).
- [75] T. Deilmann and K. S. Thygesen, *2D Mater.* **6**, 035003 (2019).
- [76] E. Malic, M. Selig, M. Feierabend, S. Brem, D. Christiansen, F. Wendler, A. Knorr, and G. Berghäuser, *Phys. Rev. Mater.* **2**, 014002 (2018).
- [77] Z. Khatibi, M. Feierabend, M. Selig, S. Brem, C. Linderälv, P. Erhart, and E. Malic, *2D Mater.* **6**, 015015 (2018).
- [78] J. Madéo, M. K. L. Man, C. Sahoo, M. Campbell, V. Pareek, E. L. Wong, A. Al-Mahboob, N. S. Chan, A. Karmakar, B. M. K. Mariserla, X. Li, T. F. Heinz, T. Cao, and K. M. Dani, *Science* **370**, 1199 (2020).
- [79] S. Dong, M. Puppin, T. Pincelli, S. Beaulieu, D. Christiansen, H. Hubener, C. W. Nicholson, R. P. Xian, M. Dendzik, Y. Deng *et al.*, *Nat. Sci.* **1**, e10010 (2021).
- [80] R. Wallauer, R. Perea-Causin, L. Münster, S. Zajusch, S. Brem, J. Güdde, K. Tanimura, K. Lin, R. Huber, E. Malic *et al.*, *Nano Lett.* **21**, 5867 (2021).
- [81] L. E. Golub, E. L. Ivchenko, and A. A. Kiselev, *J. Opt. Soc. Am. B* **13**, 1199 (1996).
- [82] R. Westphäling, S. Bauer, C. Klingshirn, A. Reznitstsky, and S. Verbin, *J. Cryst. Growth* **184–185**, 1072 (1998).
- [83] S. A. Tarasenko, A. A. Kiselev, E. L. Ivchenko, A. Dinger, M. Baldauf, C. Klingshirn, H. Kalt, S. D. Baranovskii, R. Eichmann, and P. Thomas, *Semicond. Sci. Technol.* **16**, 486 (2001).
- [84] H. Hillmer, A. Forchel, S. Hansmann, M. Morohashi, E. Lopez, H. P. Meier, and K. Ploog, *Phys. Rev. B* **39**, 10901 (1989).
- [85] K. T. Tsen, O. F. Sankey, and H. Moroc, *Appl. Phys. Lett.* **57**, 1666 (1990).
- [86] S. Shree, M. Semina, C. Robert, B. Han, T. Amand, A. Balocchi, M. Manca, E. Courtade, X. Marie, T. Taniguchi, K. Watanabe, M. M. Glazov, and B. Urbaszek, *Phys. Rev. B* **98**, 035302 (2018).
- [87] V. L. Alperovich, V. M. Zaletin, A. F. Kravchenko, and A. S. Terekhov, *Phys. Status Solidi (b)* **77**, 465 (1976).
- [88] T. Ruf, J. Spitzer, V. F. Sapega, V. I. Belitsky, M. Cardona, and K. Ploog, *Phys. Rev. B* **50**, 1792 (1994).
- [89] D. Gammon, S. Rudin, T. L. Reinecke, D. S. Katzer, and C. S. Kyono, *Phys. Rev. B* **51**, 16785 (1995).
- [90] B. Jusserand, A. N. Poddubny, A. V. Poshakinskiy, A. Fainstein, and A. Lemaitre, *Phys. Rev. Lett.* **115**, 267402 (2015).
- [91] M. Selig, G. Berghäuser, A. Raja, P. Nagler, C. Schüller, T. F. Heinz, T. Korn, A. Chernikov, E. Malic, and A. Knorr, *Nat. Commun.* **7**, 13279 (2016).
- [92] G. Wang, C. Robert, M. M. Glazov, F. Cadiz, E. Courtade, T. Amand, D. Lagarde, T. Taniguchi, K. Watanabe, B. Urbaszek, and X. Marie, *Phys. Rev. Lett.* **119**, 047401 (2017).
- [93] A. Kormányos, G. Burkard, M. Gmitra, J. Fabian, V. Zólyomi, N. D. Drummond, and V. Fal'ko, *2D Mater.* **2**, 022001 (2015).
- [94] D. Hägele, R. Zimmermann, M. Oestreich, M. R. Hofmann, W. W. Rühle, B. K. Meyer, H. Amano, and I. Akasaki, *Phys. Rev. B* **59**, R7797 (1999).
- [95] M. Kozhevnikov, B. Ashkinadze, E. Cohen, and A. Ron, *J. Lumin.* **72–74**, 312 (1997).

-
- [96] S. Rudin, T. L. Reinecke, and B. Segall, *Phys. Rev. B* **42**, 11218 (1990).
- [97] G. Moody, C. Kavir Dass, K. Hao, C.-H. Chen, L.-J. Li, A. Singh, K. Tran, G. Clark, X. Xu, G. Berghäuser, E. Malic, A. Knorr, and X. Li, *Nat. Commun.* **6**, 8315 (2015).
- [98] S. Brem, J. Zipfel, M. Selig, A. Raja, L. Waldecker, J. D. Ziegler, T. Taniguchi, K. Watanabe, A. Chernikov, and E. Malic, *Nanoscale* **11**, 12381 (2019).
- [99] H. Hillmer, S. Hansmann, A. Forchel, M. Morohashi, E. Lopez, H. P. Meier, and K. Ploog, *Appl. Phys. Lett.* **53**, 1937 (1988).
- [100] D. Oberhauser, K.-H. Pantke, J. M. Hvam, G. Weimann, and C. Klingshirn, *Phys. Rev. B* **47**, 6827 (1993).
- [101] J. T. Warren, K. E. O'Hara, and J. P. Wolfe, *Phys. Rev. B* **61**, 8215 (2000).
- [102] L. M. Smith, J. S. Preston, J. P. Wolfe, D. R. Wake, J. Klem, T. Henderson, and H. Morkoç, *Phys. Rev. B* **39**, 1862 (1989).
- [103] L. Landau and E. Lifshitz, *Physical Kinetics* (Butterworth-Heinemann, Oxford, 1981).
- [104] Z. Jin, X. Li, J. T. Mullen, and K. W. Kim, *Phys. Rev. B* **90**, 045422 (2014).